Green's Function Retrieval and Passive Imaging from Correlations of Wideband Thermal Radiations

Matthieu Davy,* Mathias Fink, and Julien de Rosny

Institut Langevin, ESPCI ParisTech, CNRS UMR 7587, 1 rue Jussieu, 75005 Paris, France

(Received 21 December 2012; revised manuscript received 8 March 2013; published 13 May 2013)

We present an experimental demonstration of electromagnetic Green's function retrieval from thermal radiations in anechoic and reverberant cavities. The Green's function between two antennas is estimated by cross correlating milliseconds of decimeter noise. We show that the temperature dependence of the cross-correlation amplitude is well predicted by the blackbody theory in the Rayleigh-Jeans limit. The effect of a nonuniform temperature distribution on the cross-correlation time symmetry is also explored. Finally, we open a new way to image scatterers using ambient thermal radiations.

DOI: 10.1103/PhysRevLett.110.203901 PACS numbers: 41.20.−q, 44.40.+a

It is a consequence of wave propagation that the field produced by a large number of uncorrelated sources is strongly correlated in time and space [1]. The Van Cittert–Zernike theorem that is extensively used by astronomers is one of the most famous illustrations of this principle. About ten years ago, Weaver and Lobkis [2,3] showed theoretically and experimentally that the Green's functions can be retrieved by cross correlating thermal ultrasonic noise in reverberant cavities.

Later this property was generalized to many other complex media [4–9]. When noise sources produce a field that is equipartitioned in energy, the time derivative of the noise correlation function at two positions is proportional to the difference between the anticausal and causal Green's functions. This result has been derived using different approaches such as modal expansion [2], reciprocity theorem [6], principle of stationary phase [7], plane wave illumination [9], and an analogy with a time reversal experiment [4,10]. For electromagnetic waves, more than 50 years ago, Rytov *et al.* predicted that in a volume in thermal equilibrium, the field cross correlation coincides with the real or imaginary part of the appropriate Green's function [11]. This result has been extended to finite geometry [12]. From a fundamental point of view, the Green's function estimation from diffuse noise cross correlations is a signature of the universal fluctuation dissipation theorem [4,11,13]. From the same theorem, it has been shown that the field autocorrelation is directly related to the local density of states which is proportional to the imaginary part of the Green's function [14]. The nonlocal density of states which measures the number of channels connecting two points can also be expressed with the spatial field cross correlation [15,16].

The Green's function estimation from diffuse noise cross correlations has paved the way for passive imaging using external noise sources because it is a way to passively estimate the transient response as if one receiver is replaced by a virtual source emitting a short pulse. Historically, it was first applied in helioseismology for measuring the travel time of acoustic waves between various points on the solar surface [17]. Later, following the work of Campillo and Paul [18], the Green's function estimation led to spectacular developments in seismology. Applying it to an entire array of seismometers makes it possible to reconstruct 2D and 3D velocity structures of Earth's crust of unprecedented high resolution [19]. The Green's function estimation from diffuse noise cross correlations has also been applied to a wide variety of other domains such as ultrasound [3,5], ocean acoustics [20], and structural monitoring [21]. Several studies have focused on detection and localization of scatterers, both theoretically [22] and experimentally [23]. At the nanometric scale, thermally excited surface plasmons have been imaged experimentally from the near-field autocorrelation [24] and numerically from the near-field degree of polarization which is given by the cross correlation of the field components [25]. The two-point cross correlation also characterizes the squeezing of the eigenmodes on disordered fractal metallic films [16].

In this Letter, we present, to our best knowledge, the first passive electromagnetic Green's function retrieval experiment in the microwave range. The last generation of fast digital oscilloscopes makes it possible to cross correlate milliseconds of microwave noise over a frequency band larger than a few GHz. Here we take advantage of ambient thermal radiations in cavities. Thermal emission at equilibrium generates a diffuse noise field, which is by nature equipartitioned and is therefore an excellent candidate for Green's function retrieval. The influence of the temperature is investigated in both an anechoic chamber and a reverberant cavity. We show that the amplitude of the cross-correlation function is consistent with blackbody theory in the Rayleigh-Jeans limit. Finally, electromagnetic Green's function estimation is applied to imaging. We show that we accurately detect and localize a metallic cylinder from measurements of ambient thermal radiations.

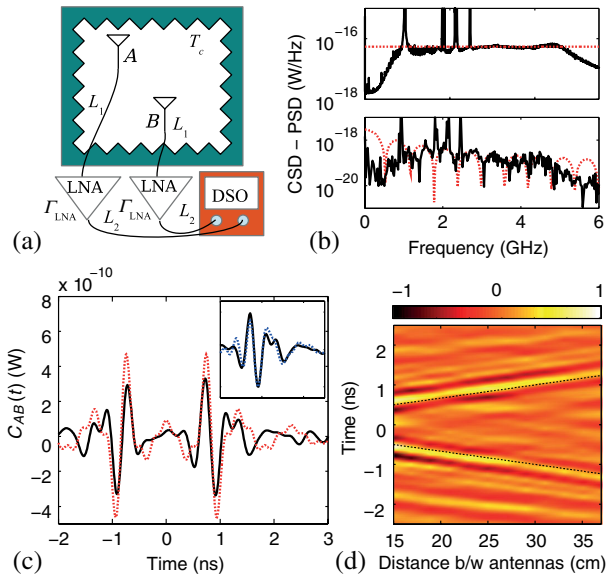

FIG. 1 (color online). (a) Schematic experimental setup. (b) Experimental (black solid line) and theoretical (red dotted line) PSD (top) and CSD (bottom) of the noise between 0.01 and 5.5 GHz. (c) Time-dependent cross correlations $C_{AB}(t)$ for a bandwidth $\Delta f = 3$ GHz between 1 and 4 GHz measured with two antennas that are 25 cm apart. In the inset, the normalized causal part of the cross correlation (black solid line) is compared to the primitive of the transient response obtained with a pulse generator (blue dotted line.). (d) Colormap representation of $C_{AB}(t)$ between -2.5 and 2.5 ns when the distance between the two antennas increases from 15 cm to 37.5 cm. The dashed line is the light cone (velocity $= 3 \times 10^8$ m/s).

The experimental setup sketched in Fig. 1(a) is made of two ultrawideband (1.7–6.0 GHz) omnidirectional antennas (MRM-UMB by Mobilemark®) connected to two low noise amplifiers [(LNA) Wenteq® ABL0400-50-4013]. We have measured a gain of $\Gamma_{\mathrm{LNA}} = 10^4$ (40 ± 1.5 dB) between 1 and 5 GHz. The noise signals are recorded on two channels of a digital sampling oscilloscope [(DSO) Tektronix® DPO71254] with a sampling rate of 25 GS/s. The first experiments are conducted in a 1 m^3 anechoic chamber. Because an anechoic chamber is made of almost perfectly absorbing walls, it behaves like an almost perfect blackbody cavity. Moreover, the radio frequency power due to strong narrow band and directive artificial sources, such as cell phones, WiFi, or Bluetooth devices is strongly attenuated inside the chamber. Those contributions would otherwise saturate the signals in our frequency range.

The power spectral density (PSD) measured by one antenna is plotted in Fig. 1(b). In contrast to the strong and narrow band contributions due to wireless communication systems [26], the thermal noise is rather flat over the bandwidth. The measured noise level N is the addition of the ambient thermal noise radiated from the walls (N_a), the intrinsic noise generated by the LNA (N_{LNA}), the noise due to losses in the coaxial cables between the antenna and the LNA (N_c), and the noise generated by the scope itself (N_s). In 1946, Dicke made the connection between the Johnson noise induced in a load and blackbody radiations recorded by a matched antenna [27]. In the Rayleigh-Jeans limit, their respective PSDs are given by [28]

$$N_a = \epsilon k_B T_c L_1 L_2 \Gamma_{\mathrm{LNA}}, \tag{1}$$

$$N_{\mathrm{LNA}} = k_B T_{\mathrm{LNA}} L_2 \Gamma_{\mathrm{LNA}}, \tag{2}$$

$$N_c = k_B T_c (1/L_1 - 1) L_1 L_2 \Gamma_{\mathrm{LNA}}, \tag{3}$$

$$N = N_a + N_{\mathrm{LNA}} + N_c + N_s. \tag{4}$$

Here k_B is the Boltzmann constant. The coefficients L_1 and L_2 due to the losses inside coax cables range from 0.6 to 0.8 depending on the wire length. The temperature $T_{\mathrm{LNA}} = 120$ K (1.5 dB noise figure) is the equivalent temperature of the noise generated by LNA. The noise PSD of the scope has been measured to be equal to 2.88×10^{-19} W/Hz at a sampling frequency of 25 GHz. Radiations from any cavity in thermal equilibrium are equal to that from a blackbody at the same temperature [29]. However, because a real system is not a perfect blackbody, the radiated noise is smaller than $k_B T_c$ by a factor ϵ, the so-called effective emissivity. In the anechoic chamber, we assume $\epsilon \sim 1$. The theoretical PSD $N = 5.4 \times 10^{-17}$ deduced from Eqs. (1)–(4) at $T_c = 298$ K is in good agreement with the experimental result plotted in Fig. 1(b).

In the following, to obtain a broadband estimation of the cross-correlation function, we record simultaneously the noise signals $n_A(t)$ and $n_B(t)$ on two antennas at positions A and B, respectively. The frequency-dependent noises $n_A(\omega)$ and $n_B(\omega)$ are the Fourier transform of 40-ns—long signals. The cross-correlation function $C_{AB}(\omega)$ is estimated from $n_A(\omega) n_B^*(\omega)$ averaged over 50 000 acquisitions. The cross-correlation spectrum density (CSD), i.e., $|C_{AB}(\omega)|$, is shown in Fig. 1(b). Since wireless contributions would dramatically degrade the estimation of the Green's function, the spectrum components that are higher than the thermal noise level are canceled. The noise cross-correlation function (NCF) $C_{AB}(t)$ is then computed from the inverse Fourier transform of $C_{AB}(\omega)$ over the bandwidth Δf. For two antennas separated by 25 cm, $C_{AB}(t)$ is plotted in Fig. 1(c). Two symmetric pulses clearly appear at -0.8 ns and 0.8 ns. This delay is equal to the travel time between the two antennas.

At thermal equilibrium, $C_{AB}(\omega)$ is proportional to the imaginary part of the Green's function between the receivers [2,8]. In case of thermal noise, this leads to

$$C_{AB}(\omega) = c_0 \Gamma_{\mathrm{LNA}} L_1 L_2 \epsilon k_B T_c \frac{G_{AB}(\omega) - G_{AB}^*(\omega)}{2i\omega}, \tag{5}$$

where c_0 is the speed of light. When $A = B$, Eq. (5) gives $C_{AB} = N_a$. Contrary to Eq. (4), the LNA, scope, and cable noises do not contribute to $C_{AB}(\omega)$ since they are

uncorrelated on the two channels of the scope. The Green's functions $G_{AB}(\omega)$ and $G^{*}_{AB}(\omega)$ correspond, respectively, to the causal and anticausal pulses that are observed in Fig. 1(c). In the anechoic chamber, because the antennas are omnidirectional and vertically polarized, $G_{AB}(\omega)$ can be approximated by the parallel-parallel component of the free-space dyadic Green's tensor of a dipole. It yields (see, e.g., Ref. [30]),

$$C_{AB}(\omega) = \alpha\Gamma_{\mathrm{LNA}}L_1L_2\epsilon k_B T_c \frac{3}{2}\left(\sin(k_0 d)\left(\frac{1}{k_0 d} - \frac{1}{(k_0 d)^3}\right) + \cos(k_0 d)\frac{1}{(k_0 d)^2}\right). \quad (6)$$

Here $k_0 = \omega/c_0$ and α is a correction factor that takes into account the mismatch between the dipole Green's function and the real one. Indeed the antenna sensitivity (gain) at 90° (i.e., perpendicular to the antenna axis) is 5 dB lower than its maximum value at 50°. Moreover, a 2.7 dB supplementary cross-correlation attenuation is consistent with antenna alignment and antenna response mismatches. These two effects imply that $\alpha \approx 0.17$. As seen in Figs. 1(b) and 1(c), the experimental results are in good agreement with Eq. (6) both in amplitude and in time dispersion. We have also directly measured the Green's function with the use of a pulse generator. We experimentally observe in Fig. 1(c) that the causal part of $C_{AB}(t)$ coincides with the primitive of the Green's function as shown by Eq. (6). One antenna is then translated over 22 cm along a rail on 12 positions. Two symmetric wave fronts associated to the causal and anticausal Green's function are clearly observed in Fig. 1(d). The two wave fronts' velocities are equal to the speed of light. The symmetry confirms the isotropy of the thermal noise radiated by the anechoic walls.

To evaluate the role of the temperature, a 70×30 cm aluminum plate covered with a carbon sheet is set in the anechoic chamber at a distance of 80 cm from antenna B. Its surface is parallel to the antennas polarization and perpendicular to a virtual line connecting the antennas. The plate temperature T_p, measured with the use of a thermal camera, slowly increases from 293 to 600 K. The cross correlation $C_{AB}(t)$ for $d = 28$ cm between the antennas is shown in Fig. 2 for two plate temperatures. Since thermal radiations of the plate illuminate the antennas from a single direction (from B to A), only the amplitude of the causal Green's function is affected by T_p. Indeed, it has been shown the contribution of noise sources to the Green's function extraction strongly depends on the source directions [5,31]. In our case, the noise that contributes to the retrieved causal Green's function mainly arises from the hot plate area. The amplitude increases linearly with T_p as seen in Fig. 2(b). A good approximation of the causal Green's function amplitude can be found when T_c in Eq. (6) is replaced by $\epsilon_p T_p + (1 - \epsilon_p)T_c$. Here ϵ_p is the emissivity of the plate. According to Kirchoff's law of thermal radiation, the emissivity ϵ_p is equal to its absorptivity α_p. From active measurements of the intensity transmitted and reflected by the plate, we have found $\alpha_p = 0.13$, which is in good agreement with $\epsilon_p = 0.15$ deduced from a linear fit of the data in Fig. 2(b). All these results confirm the thermal origin of $C_{AB}(t)$.

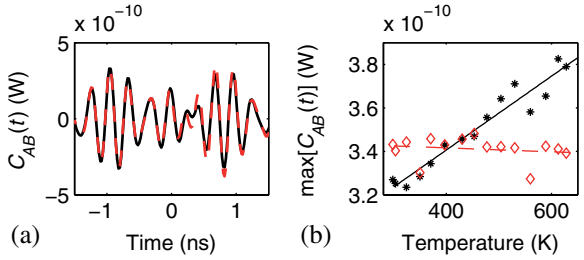

FIG. 2 (color online). (a) Cross correlation $C_{AB}(t)$ for $\Delta f = 1.5$ GHz between two antennas that are 25 cm apart when the temperature of the plate is $T_p = 298$ K (black solid line) and $T_p = 600$ K (red dashed line). (b) The maxima of the causal (asterisk) and anticausal (open diamond) parts of $C_{AB}(t)$ are plotted with T_p. The black and red dotted lines are linear fits of the data. At ambient temperature, the two pulses are not perfectly symmetric due to a small noise anisotropy.

Noise cross correlations are now investigated in an oven that acts as a reverberant cavity at microwave frequency range. The noise is recorded in a 0.25 m^3 oven with stainless steel walls, located in the anechoic chamber. As a reference, we first measure the PSD of the noise generated by an Ohmic load (50 Ω). The temperature of the oven T_o probed by a thermocouple in contact with the 50 Ω load ranges from 298 to 370 K. The PSD of this Johnson-Nyquist noise is in good agreement with $k_B T_o$ in Fig. 3(a). The Ohmic load is then replaced by a single omnidirectional antenna, and the thermocouple probes the temperature of the steel walls. At ambient temperature ($T_o = T_c$), the system made of the oven and the anechoic chamber is in thermal equilibrium, and the thermal noise level is given by $k_B T_c$. However, when T_o increases, the temperatures of the oven and the cavity differ. The noise level is then given by $k_B(T_c + \epsilon_o[T_o - T_c])$, where the emissivity of the oven ϵ_o is smaller than 1 due to radiative losses. The PSD is seen to increase linearly with T_o in Fig. 3(a), and a good fit of the data is obtained with $\epsilon_o = 0.6$.

The cross correlation $C_{AB}(t)$ measured between two omnidirectional antennas that are 20 cm apart is presented in Fig. 3(b). Because of multiple reflections occurring on the oven walls, the signal spreads over 10's of nanoseconds. Even in such a complex medium, we obtain a good estimation of the Green's function over more than 10 ns. The maximum amplitude of $C_{AB}(t)$ corresponding to the direct path between the antenna grows linearly with T_o in Fig. 3(c) and is in good agreement with Eq. (6) in which T_o is replaced by $T_c + \epsilon_o(T_o - T_c)$.

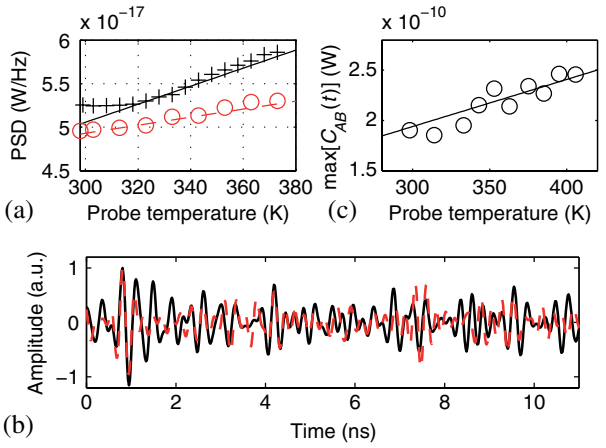

FIG. 3 (color online). (a) Temperature dependence of the PSD of a 50 Ω resistor load (plusses) and an omnidirectional antenna (open circle). The continuous black line and the red dotted line are the respective theoretical PSDs. (b) The causal part of $C_{AB}(t)$ between two antennas that are 20 cm apart inside the oven at 298 K (black solid line) is compared to the primitive of the transient response (red dashed line) measured actively. (c) Maximum of the cross correlation as a function of T_o. The black line is the theoretical prediction using Eq. (5) in which T_c is replaced by $T_c + \epsilon_o(T_o - T_c)$.

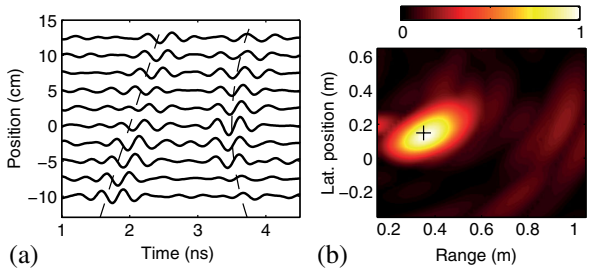

FIG. 4 (color online). (a) Seismiclike representation of the causal part of ten cross correlations recorded on two horn antennas with a 5-cm diameter metallic cylinder located at a range of 35 cm. The cross correlations are obtained for ten positions of antenna B while antenna A is fixed, so that the synthetic array is 22.5 cm long. (b) Normalized image obtained from beamforming of $C_{AB}(t)$. The black cross is the actual location of the scatterer.

Finally, the Green's function retrieval from thermal noise is applied to imaging. Here we use the field scattered by an object to detect and localize it. Two small wideband horn antennas in the anechoic chamber are pointed toward the area of interest where a scatterer stands, so that the scattered wave is enhanced compared to the direct path contributions. A synthetic array with a total aperture of 22.5 cm is created by moving antenna B over ten positions. The scatterer is a 5-cm diameter aluminum cylinder parallel to the antenna's polarization. In Fig. 4(a), we clearly observe two wave fronts on the ten cross-correlation acquisitions filtered between 2 and 4 GHz. The first one is associated to the direct path between the two antennas and the second one to the wave scattered off the cylinder. An image is then built with standard array processing (time delay beamforming) applied to the difference of the retrieved Green's functions with and without the scatterer [32]. The brightest spot shown in Fig. 4(b) clearly appears at the scatterer location. Because the target is close to the virtual array, the lateral resolution approximately equals one central frequency wavelength, i.e., 10 cm at 3 GHz. As for the range resolution, it is given by $c_0/2\Delta f$ which depends on inverse of the bandwidth Δf. In our case, the experimental resolution (10 cm) is a little bit larger than the theoretical one (7.5 cm). We have therefore created a thermal emission detection and ranging (THEDAR), which consists of an ultrawideband passive radar based on thermal noise diffuse field. This completely differs from narrow band passive radar systems at microwave frequencies which exploit "illuminators of opportunity," such as broadcast emitters (radio, TV) [33] or wireless networks (GSM, WiFi, Bluetooth, etc.) [34]. Here, thanks to the diffuse property of thermal noise, the imaging device only weakly depends on the emission properties of the thermal source.

In conclusion, we have experimentally retrieved the Green's function from wideband diffuse thermal noise in the microwave range. This has been achieved by computing the averaged cross correlation of microwave noise signals. The amplitude of the cross correlation has been shown to increase with the temperature in agreement with thermal noise laws. An original application to passive wideband imaging has also been demonstrated. Because the noise power spectrum distribution follows Planck's law which is maximum at a wavelength of about 10 μm at ambient temperature, it would be of great interest to transpose the passive estimation of the Green's function to the long-wavelength infrared range. Finally, we can even imagine to retrieve the stellar Green's functions with echoes due to the reflection off stellar bodies from the cross correlation of the cosmic microwave background radiation at 2.7 K.

We are grateful to Fonds ESPCI-Georges Charpak and Direction Générale de l'Armement who partially funded this work.

*Present address: Institut d'Electronique et de Télécommunications de Rennes, University of Rennes 1, F-35042 Rennes, France.

[1] J. Goodman, *Statistical Optics: An Introduction* (Wiley, New York, 1984).
[2] R. L. Weaver and O. I. Lobkis, Phys. Rev. Lett. **87**, 134301 (2001).
[3] R. Weaver and O. Lobkis, Ultrasonics **40**, 435 (2002).
[4] B. A. van Tiggelen, Phys. Rev. Lett. **91**, 243904 (2003).
[5] A. Derode, E. Larose, M. Campillo, and M. Fink, Appl. Phys. Lett. **83**, 3054 (2003).
[6] K. Wapenaar, Phys. Rev. Lett. **93**, 254301 (2004).

[7] R. Snieder, Phys. Rev. E **69**, 046610 (2004).
[8] K. Wapenaar, E. Slob, and R. Snieder, Phys. Rev. Lett. **97**, 234301 (2006).
[9] F. J. Sanchez-Sesma, J. A. Perez-Ruiz, M. Campillo, and F. Luzon, Geophys. Res. Lett. **33**, L13305 (2006).
[10] A. Derode, E. Larose, M. Tanter, J. de Rosny, A. Tourin, M. Campillo, and M. Fink, J. Acoust. Soc. Am. **113**, 2973 (2003).
[11] S. Rytov, I. Kravtsov, and V. Tatarskii, *Principles of Statistical Radiophysics 3: Elements of Random Fields* (Springer-Verlag, Berlin, 1989).
[12] G. S. Agarwal, Phys. Rev. A **11**, 230 (1975).
[13] H. Callen and T. Welton, Phys. Rev. **83**, 34 (1951).
[14] K. Joulain, R. Carminati, J.-P. Mulet, and J.-J. Greffet, Phys. Rev. B **68**, 245405 (2003).
[15] E. Akkermans and G. Montambaux, *Mesoscopic Physics of Electrons and Photons* (Cambridge University Press, Cambridge, England, 2007).
[16] A. Cazé, R. Pierrat, and R. Carminati, Phys. Rev. Lett. **110**, 063903 (2013).
[17] T. Duvall, S. Jefferies, J. Harvey, and M. Pomerantz, Nature (London) **362**, 430 (1993).
[18] M. Campillo and A. Paul, Science **299**, 547 (2003).
[19] N. Shapiro, M. Campillo, L. Stehly, and M. Ritzwoller, Science **307**, 1615 (2005).
[20] P. Roux, W. Kuperman, and N. Grp, J. Acoust. Soc. Am. **116**, 1995 (2004).
[21] E. Larose, T. Planes, V. Rossetto, and L. Margerin, Appl. Phys. Lett. **96**, 204101 (2010).
[22] R. Snieder, F. J. Sanchez-Sesma, and K. Wapenaar, SIAM J. Imaging Sci. **2**, 763 (2009).
[23] E. Larose, G. Montaldo, A. Derode, and M. Campillo, Appl. Phys. Lett. **88**, 104103 (2006).
[24] Y. De Wilde, F. Formanek, R. Carminati, B. Gralak, P.-A. Lemoine, K. Joulain, J.-P. Mulet, Y. Chen, and J.-J. Greffet, Nature (London) **444**, 740 (2006).
[25] V. Yannopapas and N. V. Vitanov, Phys. Rev. B **80**, 035410 (2009).
[26] The three narrow peaks close to 900, 1900, 2100 MHz are due to GSM or UMTS systems (mobile phones) and the last one at 2450 MHz is due to WiFi devices.
[27] R. Dicke, Rev. Sci. Instrum. **17**, 268 (1946).
[28] S. J. Orfanidis, "Electromagnetic Waves and Antennas" (unpublished).
[29] M. Zemansky and R. Dittman, *Heat and Thermodynamics* (McGraw-Hill, New York, 1981).
[30] J. de Rosny, G. Lerosey, and M. Fink, IEEE Trans. Antennas Propag. **58**, 3139 (2010).
[31] P. Roux, K. G. Sabra, W. A. Kuperman, and A. Roux, J. Acoust. Soc. Am. **117**, 79 (2005).
[32] The image intensity at position $\boldsymbol{r}$ is formed by coherent summation of the difference between the cross correlations measured with and without the metallic cylinder $[\delta C_{AB_i}(t)]$. More precisely, the image intensity $I(\boldsymbol{r})$ at position $\boldsymbol{r}$ is given by $\int_{t=-\delta t}^{\delta t} |\sum_i \delta C_{AB_i}(t - c_0^{-1}(\|\boldsymbol{r}_A - \boldsymbol{r}\| + \|\boldsymbol{r}_{B_i} - \boldsymbol{r}\|))|^2 dt$, where $\boldsymbol{r}_{B_i}$ is the position of antenna B for the ith measurement, c_0 is the speed of light, and δt is an integration time that is given by the inverse of the bandwidth. Hence, before performing a coherent sum over the positions of antenna B, $\delta C_{AB_i}(t)$ is time delayed to compensate the travel time for the wave to go from antenna A to position $\boldsymbol{r}$ and come back to antenna B_i.
[33] H. Griffiths and N. Long, IEEE Proc. Rad. Signal Process **133**, 649 (1986).
[34] D. Tan, H. Sun, Y. Lu, M. Lesturgie, and H. Chan, IEEE Proc. Rad. Sonics Nav. **152**, 116 (2005).